Dynamic inland propagation of thinning due to ice loss at the margins of the Greenland ice sheet

Weili WANG,[1] Jun LI,[1] H. Jay ZWALLY[2]

[1]SGT Inc., NASA Goddard Space Flight Center, Greenbelt, MD, USA
E-mail: weili.wang@nasa.gov
[2]Cryospheric Sciences Branch, NASA Goddard Space Flight Center, Greenbelt, MD, USA

ABSTRACT. Mass-balance analysis of the Greenland ice sheet based on surface elevation changes observed by the European Remote-sensing Satellite (ERS) (1992–2002) and Ice, Cloud and land Elevation Satellite (ICESat) (2003–07) indicates that the strongly increased mass loss at lower elevations (<2000 m) of the ice sheet, as observed during 2003–07, appears to induce interior ice thinning at higher elevations. In this paper, we perform a perturbation experiment with a three-dimensional anisotropic ice-flow model (AIF model) to investigate this upstream propagation. Observed thinning rates in the regions below 2000 m elevation are used as perturbation inputs. The model runs with perturbation for 10 years show that the extensive mass loss at the ice-sheet margins does in fact cause interior thinning on short timescales (i.e. decadal). The modeled pattern of thinning over the ice sheet agrees with the observations, which implies that the strong mass loss since the early 2000s at low elevations has had a dynamic impact on the entire ice sheet. The modeling results also suggest that even if the large mass loss at the margins stopped, the interior ice sheet would continue thinning for 300 years and would take thousands of years for full dynamic recovery.

INTRODUCTION

In contrast to a near-balance status in the 1990s (Zwally and others, 2005), the Greenland ice sheet (GIS) has experienced a marked mass loss (171 Gt a^{-1}) since the early 2000s (Zwally and others, 2011). Substantial losses occurred at low elevations due to extensive surface melt and dynamic thinning at the margins (Zwally and others, 2011), particularly in the outlet glaciers as a result of accelerated flow (Howat and others, 2007; Pritchard and others, 2009) and surface melting (Mernild and others, 2009). Although the inland portion of the GIS continued to grow from the 1990s due to the increased accumulation rate, the mass gain above 2000 m elevation has decreased since the 2000s (table 1 of Zwally and others, 2011). After correction for enhanced firn compaction due to surface warming (which lowers the surface elevation) and bedrock motion, the approximate change in thickness of the ice column (dI/dt) was nearly unchanged during 2003–07 compared with the 1990s. However, an increase in surface elevation (dH^a_{CA}/dt) at higher elevations due to the increase in accumulation was approximately balanced by an increase in dynamic thinning (dH_{bd}/dt) that also extended to higher elevations (fig. 10 in Zwally and others, 2011). Those results suggest that increased melting and strong dynamic thinning initiated at the margins propagates rapidly into the high elevations of the ice-sheet interior in some drainage systems (Fig. 1a).

Previous modeling studies have found that the thinning and acceleration initiated by the change in boundary conditions at the ice terminus propagate inland (Parizek and Alley, 2004; Payne and others, 2004; Price and others, 2008a,b, 2011; Nick and others, 2009; Joughin and others, 2010). Most studies focused on the locally fast flow region or the dynamic changes in a short time period.

In this paper, we examine the time response of the GIS to elevation perturbations at the margins using a three-dimensional (3-D) ice-flow model that incorporates anisotropic ice flow. The perturbation experiment is conducted using rates of thinning at lower elevations derived from the European Remote-sensing Satellite (ERS) and Ice, Cloud and land Elevation Satellite (ICESat) as the perturbation input to investigate the impacts of the recent strong mass losses at the margins on the interior of the ice sheet.

Numerical model

A 3-D time-dependent Anisotropic Ice-Flow model (AIF model) incorporating anisotropic ice flow was developed, which fully couples dynamics and thermodynamics. This is a higher-order model with longitudinal and vertical shear stresses. The model calculates ice-sheet thickness, distributions of stress, velocity, temperature and flow properties throughout. In Cartesian coordinates (x, y, z), i denotes x and y, and j denotes z. The ice thickness is calculated based on the continuity equation:

$$\frac{\partial H}{\partial t} = -\nabla \cdot (\vec{V}_i H) + B - M, \quad (1)$$

where $\frac{\partial H}{\partial t}$ is the change in ice thickness H with time t. B is the net surface mass balance taken as the present-day constant (updated from Zwally and Giovinetto, 2000). M is the basal melting rate. $\bar{V}_i$ is the depth-averaged horizontal velocity, V_i:

$$V_i = 2\int_0^z \dot{\varepsilon}_{ij}\,dz + V_b i. \quad (2)$$

$\dot{\varepsilon}_{ij}$ is the shear strain rate. The basal sliding velocity V_b and basal melting rate M are calculated based on the basal shear stress, $\tau_b = -\rho g H \alpha$, as

$$V_b = A_s \frac{\tau_b^3}{Z^*}, \quad (3)$$

$$M = \frac{V_b \tau_b}{\rho L_f}, \quad (4)$$

where A_s is a constant (Wang and others, 2002a), Z^* is the

https://doi.org/10.3189/2012JoG11J187 Published online by Cambridge University Press

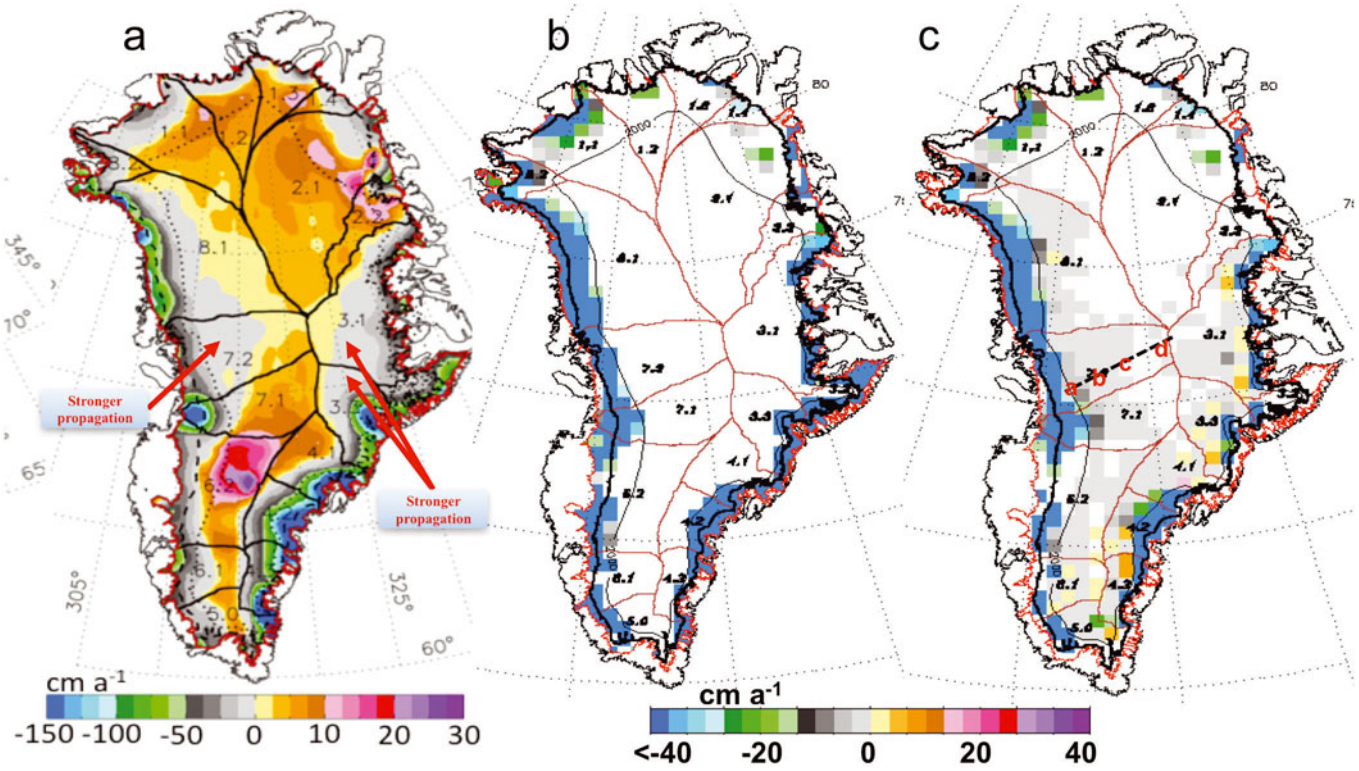

Fig. 1. Greenland ice sheet thickness changes. (a) Dynamic thickness changes from ICESat observation (fig. 7b in Zwally and others, 2011), dH_{bd}/dt, include both ablation and dynamic terms below the equilibrium line and only dynamic terms above the equilibrium line. The stronger propagation regions where the dynamic thinning extends inland in drainage systems 3 and 7 are indicated. (b) Model perturbation input: the difference in dynamic thickness changes (<2000 m elevation) between ICESat (2003–07) and ERS (1992–2002) observations. (c) Modeled results after 10 year perturbation, showing agreement with the observations in (a) that enhanced inland thinning occurs mainly in the western, eastern and southeastern regions of the ice sheet. Results for four locations along the flowline (dashed line) marked a, b, c and d are presented in Figure 3. The 2000 m contour is shown as a dotted line in (a) and a thin solid line in (b) and (c). The equilibrium line is shown as a dashed line in (a) and a thick solid line in (b) and (c).

height above buoyancy, L_f is the latent heat of fusion of ice (Price and others, 2008b), ρ is the density of ice, g is the acceleration due to gravity and α is the surface slope. The parameters are presented in Table 1. V_b and M occur when the basal temperature reaches the pressure-melting point (Eqns (9) and (10)).

A successful ice-sheet model relies on an accurate specification of the flow law that governs the flow behavior of ice. Most ice-sheet models use a form of Glen's flow law (Glen, 1958), which is not appropriate when anisotropy of the ice crystal fabric develops in the deeper parts of the ice sheet. Using the flow law for isotropic ice (Glen's law) leads to a flow velocity three to eight times less than observed values. Most ice-sheet models simply use a constant enhancement factor of 3 or 5 (e.g. Huybrechts and others, 1991; Hvidberg and others, 1997) to account for this discrepancy. Some attempts have been made to describe the anisotropic ice flow by incorporating the effects of anisotropy into the constitutive relation (e.g. Azuma and Goto-Azuma, 1996; Greve and others, 2009). Alternatively, Glen's flow law can be modified to include anisotropic effects by introducing an enhancement factor defined as the ratio of the strain rate for anisotropic ice to the strain rate for isotropic ice, where an increase in the enhancement factor is associated with a strengthening of a near-vertical single-maximum fabric (e.g. Dahl-Jensen, 1985; Wang and Warner, 1999).

To provide reliable estimates of evolving ice-sheet geometry, the treatment of the flow of ice needs to be based on a proper understanding of ice rheology. In this model, we use the flow law from a previous study (Wang and Warner, 1999):

$$\dot{\varepsilon}_{ij}^{n} - E(\lambda_c)A(T)\tau_{ij}^{n}(\dot{\varepsilon}_{ij}^{n-1} + \dot{\varepsilon}_{ii}^{n-1}) = 0. \quad (5)$$

Enhancement factor $E(\lambda_c)$, derived from laboratory measurements of ice rheology (Li and others, 1996), accounts for the effect of anisotropy for ice:

$$E(\lambda_c) = E_s(E_c/E_s)^{\lambda_c}, \quad (6)$$

Table 1. Physical parameters used in the model

Symbol	Parameter	Value	Unit
A_0	Temperature parameter ($T \leq 263$)	1.14×10^{-5}	$Pa^{-3}\,a^{-3}$
A_0	Temperature parameter ($T > 263$)	5.47×10^{10}	$Pa^{-3}\,a^{-3}$
A_s	Sliding parameter	2.0×10^{-11}	$m^2\,Pa^{-3}\,a^{-1}$
c	Specific heat of ice	$152.5 + 7.12T$	$J\,kg^{-1}\,K^{-1}$
g	Gravity acceleration	9.81	$m\,s^{-2}$
k	Thermal conductivity of ice	$9.828e^{-0.0057T}$	$W\,m^{-1}\,K^{-1}$
L_f	Latent heat of fusion of ice	333.5	$kJ\,kg^{-1}$
n	Flow law exponent	3	–
Q	Activation energy ($T \leq 263$)	60	$kJ\,mol^{-1}$
Q	Activation energy ($T > 263$)	139	$kJ\,mol^{-1}$
R	Universal gas constant	8.314	$J\,mol^{-1}\,K^{-1}$
ρ	Density of ice	910	$kg\,m^{-3}$
G	Basal geothermal heat flux	–0.07	$W\,m^{-2}$

https://doi.org/10.3189/2012JoG11J187 Published online by Cambridge University Press

where

$$\lambda_c = \tau_{ii}/\sqrt{\tau_{ij}^2 + \tau_{ii}^2} \quad \text{or} \quad \lambda_c = \dot{\varepsilon}_{ii}/\sqrt{\dot{\varepsilon}_{ij}^2 + \dot{\varepsilon}_{ii}^2} \tag{7}$$

is a function of stress configurations. $E_s = 10$ and $E_c = 3$ are respective enhancement factors for shear or compression alone. As λ_c varies with ice-sheet depth from 1 to 0 as the stress situation varies from vertical compression (or longitudinal extension, i.e. $\tau_{ij} = 0$) to simple shear (i.e. $\tau_{ii} = 0$), the enhancement factor increases from 3 to 10, corresponding to ice fabric changes from a small-circle girdle pattern to a single-maximum pattern. Previous applications of this enhancement factor have successfully described the flow behavior of ice (e.g. Wang and Warner, 1999; Wang and others, 2002a; Breuer and others, 2006; Price and others, 2007).

The temperature parameter $A(T)$ is taken as the Arrhenius relation (Paterson, 1994):

$$A(T) = A_o \exp\left(-\frac{Q}{RT}\right), \tag{8}$$

where A_o is a constant, R is the universal gas constant and Q is the activation energy for ice creep (Table 1). By assuming that the temperature gradients in horizontal directions are very small compared with the vertical gradient, the temperature T is calculated from the equation for heat transfer:

$$\frac{\partial T}{\partial t} = \frac{k}{\rho c}\frac{\partial T^2}{\partial X_j^2} + \frac{1}{\rho c}\frac{\partial k}{\partial T}\left(\frac{\partial T}{\partial X_j}\right)^2 - \vec{V}_i \cdot \nabla T - w\frac{\partial T}{\partial X_j} + q, \tag{9}$$

where c is specific heat of ice and k is the thermal conductivity of ice (Table 1). $q = 2\tau_{ij}\dot{\varepsilon}_{ij}/\rho c$ is the internal heating due to the deformation. The vertical velocity w can be obtained from the horizontal velocities (Eqn (2)) based on the assumption that ice is incompressible.

Two boundary conditions are required to solve Eqn (9). At the surface, the temperature is taken from the model input. At the base, the temperature is determined as

$$\begin{aligned} T &= T_{pmp} \qquad (T \geq T_{pmp}) \\ \frac{\partial T}{\partial X_j} &= \frac{G}{k} \qquad (T < T_{pmp}) \end{aligned} \tag{10}$$

T_{pmp} is the pressure-melting point. G is the basal geothermal heat flux (Table 1).

The shear stress τ_{ij} is calculated in terms of ice density ρ, the acceleration due to gravity g, the depth h and the surface slope α_i:

$$\tau_{ij} = -\rho g h \alpha_i. \tag{11}$$

In Eqn (5) the longitudinal strain rate ($\dot{\varepsilon}_{ii}$) is involved in the shear strain rate ($\dot{\varepsilon}_{ij}$) to take account of the variations of flow properties and stresses along ice flow. The longitudinal strain rate is the gradient of the horizontal velocity

$$\dot{\varepsilon}_{ii} = \frac{\partial V_i}{\partial X_i}. \tag{12}$$

It can be expressed as

$$\begin{aligned} \frac{\partial V_i}{\partial X_i} = &\frac{\partial}{\partial X_i}\left[\int_0^z 2E(\lambda_c)A(T)\tau_{ij}^n \, dz\right] \\ &+ \frac{\partial}{\partial X_i}\left[\int_0^z 2E(\lambda_c)A(T)\tau_{ii}^{n-1}\tau_{ij} \, dz\right], \end{aligned} \tag{13}$$

which indicates that the flow law (Eqn (5)) also includes the effect of the shear stress and the longitudinal stress gradients which are considered to play an important role at some places in the ice sheet, such as the areas of rough bedrock, fast ice flow or ice divides (Budd, 1971; Pattyn and others, 2008). If $\dot{\varepsilon}_{ii}$ is not included in Eqn (5) the flow law simplifies to a shallow-ice approximation form (Hutter, 1983):

$$\dot{\varepsilon}_{ij} = E(\lambda_c)A(T)\tau_{ij}^n. \tag{14}$$

In this study we used the anisotropic ice flow law (Eqn (5)) and Eqns (1–12) to solve the ice thickness, shear and longitudinal strain rates, enhancement factors, temperatures, velocities, shear and longitudinal stresses.

PERTURBATION EXPERIMENT

The perturbations are taken from the difference of the ice-thickness changes (dH_{bd}/dt) below 2000 m elevation between ICESat (2003–07) and ERS (1992–2002), which represent the thickness change since 2003 (Zwally and others, 2011). dH_{bd}/dt includes the combined dynamic and ablation terms ($dH_{bd}/dt \equiv dH_d/dt + dH_b/dt$). In the ablation zone, dH_{bd}/dt includes contributions from both ice dynamics (dH_d/dt) and melt (dH_b/dt). In the accumulation zone, dH_{bd}/dt contains only the dynamic term (Li and Zwally, 2011). The decrease of dH_{bd}/dt above 2000 m is considered to be a result of the inland propagation from the mass loss at lower elevations of the ice sheet. At some locations (mainly in the north) the perturbations are small and positive, which would cause dynamic thickening. To emphasize the stronger dominant impacts of the mass losses, we only use the gridpoints with negative perturbations. All positive perturbations are set to zero (Fig. 1b).

The experiment is intended to answer two questions: (1) How far and how rapidly will the strong mass loss from the coastal regions propagate inland? (2) How many years will the impact remain?

We set up the modeling runs in three steps. The first step is to establish a steady-state ice sheet which corresponds to present-day conditions (Fig. 2), using the present-day basal topography (Bamber and others, 2001), surface mass balance (updated from Zwally and Giovinetto, 2000), surface temperature and balance velocity. Derived balance velocity is based on the ICESat observed thickness (http://nsidc.org/data/nsidc-0304.html) and present-day surface mass balance using the scheme from Budd and Warner (1996). To establish the present-day steady-state ice sheet (Fig. 2b and d), the model iterates on the governing equations (Wang and Warner, 1999), with the balance velocity (Fig. 2c) as a target. To compensate for any overestimated velocity without tuning any parameter in the flow law, we adopted the scheme from Wang and Warner (1999) by discounting integration of shear strain rate near the base of the ice sheet to match the balance velocity (Fig. 2c). This treatment produces strain-rate profiles with a band of high shear above the bedrock which can be compared with observations (e.g. Wang and Warner, 1999, fig. 3; Wang and others, 2002b, fig. 4).

In the second step, we put in the perturbations (Fig. 1b) and run the model for 10 years. The modeled results are compared with the observations (dH_{bd}/dt). The third step is set up to answer the question of how many years the impact is sustained after the perturbations are switched off by running the model forward 100 ka. The surface mass balance and temperature remain unchanged, which allows us to examine the impact from an isolated 10 year

https://doi.org/10.3189/2012JoG11J187 Published online by Cambridge University Press

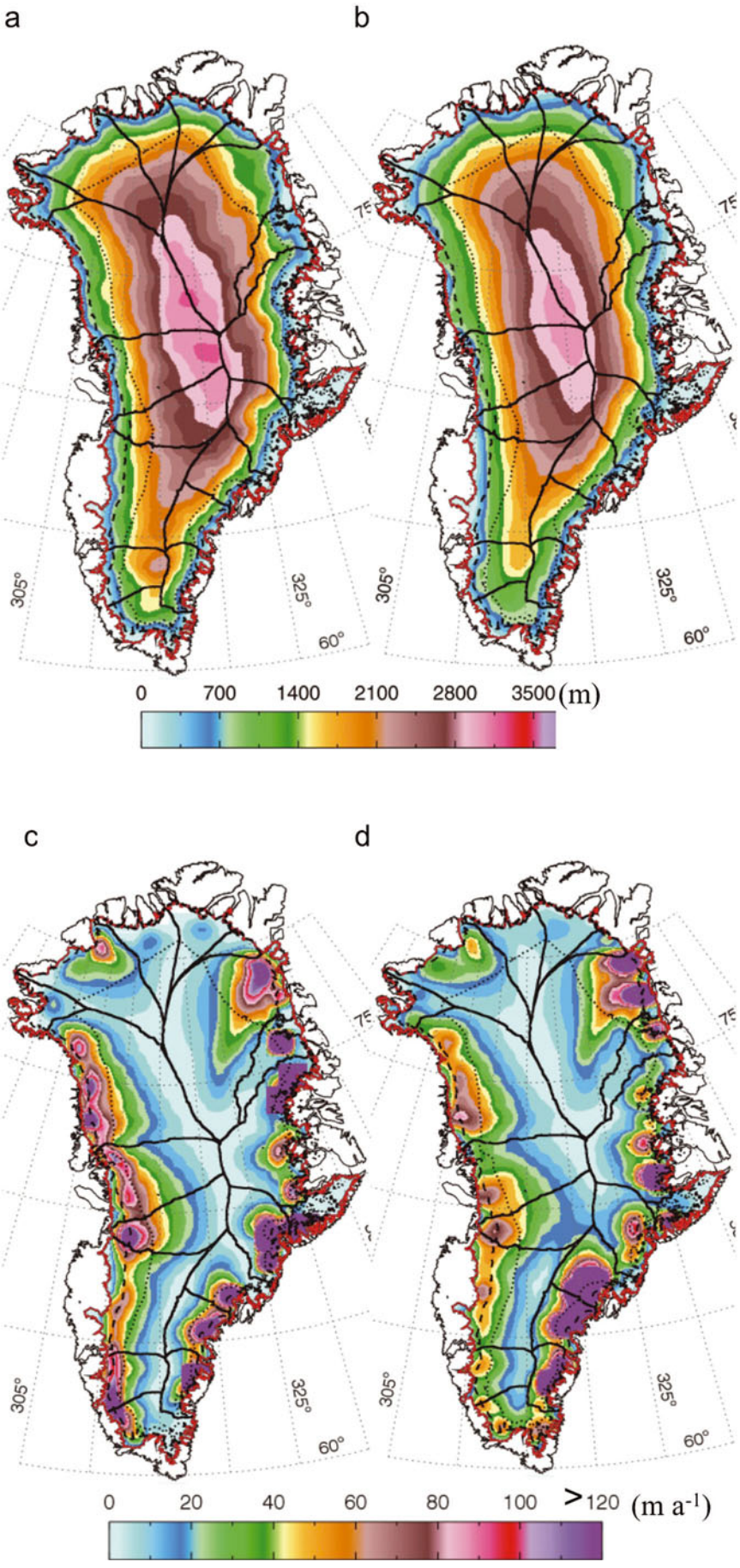

Fig. 2. Initial state of the Greenland ice sheet for perturbation experiment. (a) Thickness derived from ICESat observation (http://nsidc.org/data/nsidc-0304.html). (b) Modeled thickness. (c) Derived balance velocity based on the ICESat observed thickness and present-day surface mass balance. (d) Modeled depth-averaged horizontal velocity. The 2000 m contour and equilibrium line are shown as a dotted line and dashed line, respectively.

https://doi.org/10.3189/2012JoG11J187 Published online by Cambridge University Press

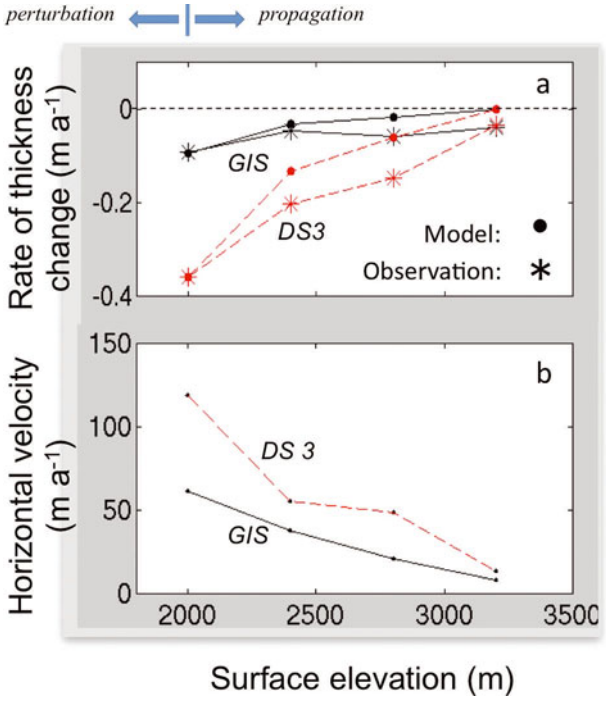

Fig. 3. (a) The rate of ice-thickness change averaged in 400 m elevation bands over the ice sheet versus elevations from the observations and the modeled results after 10 year perturbation (Fig. 1c) over the whole ice sheet (GIS, black solid line) and drainage system 3 (DS3, red dashed line) which shows the stronger propagation. (b) Corresponding depth-averaged horizontal velocities. The ranges of perturbation (<2000 m elevation) and propagation (>2000 m elevation) are shown by the arrows.

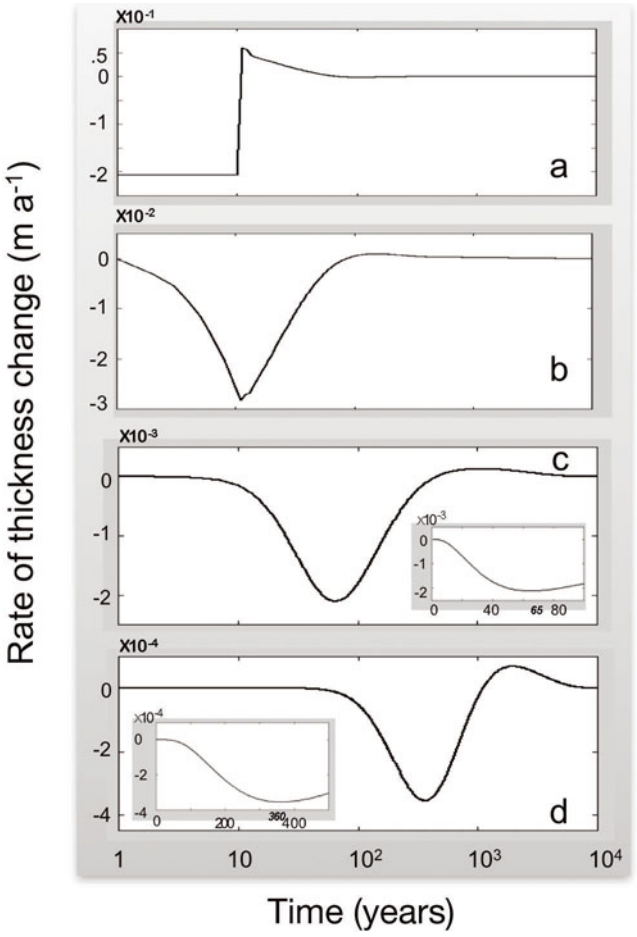

Fig. 4. Modeled ice-thickness changes with time (log scale) at four selected locations along the flowline in West Greenland (see Fig. 1c): (a) at the perturbation region; (b–d) at ~100 km (b), ~200 km (c) and ~400 km (d) upstream from the perturbation region. The insets in (c) and (d) plot the time using a linear scale to show the time when the maximum thinning rates are reached.

perturbation of the thickness. The model does not include an ice-front calving process. dH_{bd}/dt is small and the total thinning for a 10 year perturbation at any perturbation gridpoint is a small portion of the thickness. Therefore, we treat the marginal ice edge as steady-state during the experimental period.

The model has a horizontal resolution of 50 km, compatible with the resolution of the observations, and 31 evenly spaced vertical layers. The time-steps are 1 year. The physical parameters used in the model are listed in Table 1. A finite-difference technique is used to solve the equations.

RESULTS AND DISCUSSION

The modeled results after 10 years of perturbation input show that the observed strong mass loss at low elevations certainly causes interior ice-sheet thinning (Figs 1c and 3a). The dynamic propagation penetrates deep into the ice sheet, to almost the highest elevations. The modeled thinning pattern (Fig. 1c) over the ice sheet is in agreement with the observations (Fig. 1a), showing that enhanced thinning mainly occurs in the west and east, as well as in the southeast. In contrast, the thinning is least in the north and southwest. This implies that satellite-observed thinning (or reduced thickening) in the higher elevations of the ice sheet is likely induced by the extensive mass loss at the margins during the past decade or so.

The stronger propagation (Fig. 3a) corresponding to the higher horizontal velocities (Fig. 3b) in drainage system 3 indicates that faster ice flow enhances the propagation. The lack of resolution of basal troughs at 50 km grid spacing may result in reducing the speed of the propagation, as the deep troughs lead to higher driving stresses and warmer ice and therefore faster ice flow and stronger propagation. Improvement of the modeling spatial and temporal resolutions may enhance the propagation and reduce the discrepancies in the thinning rates between the modeled results and the observations (Fig. 3a).

After the perturbations are switched off, the ice sheet in the perturbation region starts to grow at a very high rate and then slowly returns to the previous steady state (Fig. 4a), while the ice sheet in the propagation region keeps thinning before recovering (Fig. 4b–d). The maximum thinning rates occur after 1, 55 and 350 years (i.e. years 11, 65 and 360 in Fig. 4b–d) at 100, 200 and 400 km upstream, respectively, showing a propagation wave: the farther from the perturbation region, the later the response occurs. The thickening rates during the recovery period are low compared with the ice loss rates during the period of thinning, so the ice sheet takes longer to return to its pre-perturbation state than it did to reach the thinnest state.

The changes in ice-sheet mass through time (Fig. 5) show the impact of the 10 year perturbations. In the first 10 years, the interior of the ice sheet (propagation region shown as red

https://doi.org/10.3189/2012JoG11J187 Published online by Cambridge University Press

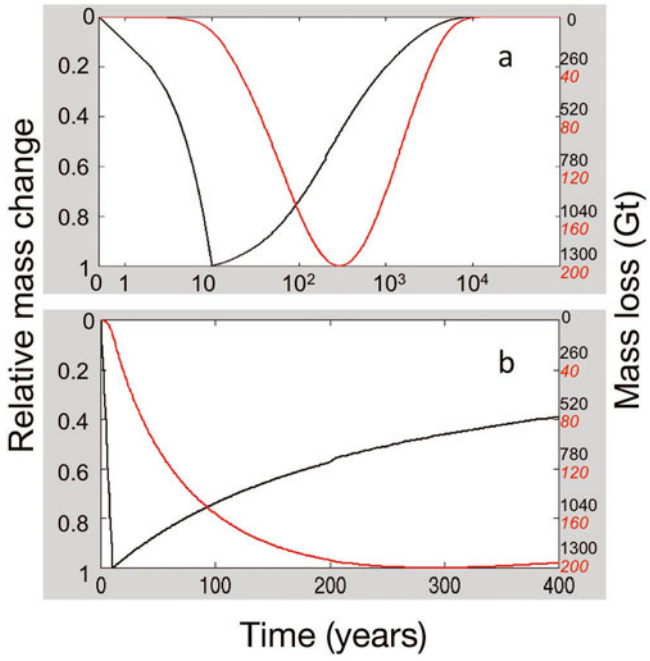

Fig. 5. Modeled ice-sheet mass change over the whole ice sheet (black line) and the ice sheet above 2000 m elevation (red line) as a function of time (a) in log scale for 10 ka and (b) in linear scale for the first 400 years, showing the times when the maximum mass losses are reached. The left-hand labels indicate the mass change relative to the maximum mass loss. The right-hand labels indicate the total mass loss (Gt) from the steady state for the whole ice sheet (black numbers) and for the ice sheet above 2000 m elevation (red numbers).

line) starts thinning slowly through the dynamic propagation along with a rapid mass loss over the whole ice sheet (black line) mainly due to the applied perturbations. While the whole ice sheet starts to grow back from the 11th year, when the perturbations are switched off at a total mass loss of 1300 Gt, the interior ice sheet keeps thinning until ~300 years due to dynamic propagation. After reaching the maximum mass loss of 200 Gt, the interior ice sheet also starts thickening. Both the interior and low-elevation regions reach the steady state again at ~10 ka. Figure 5 illustrates that the strongest impact of the 10 year perturbations on the interior ice sheet occurs at ~300 years and the impact is sustained for 10 ka until full ice-sheet dynamic recovery. This result indicates that even if the large mass losses at the margins of the GIS ended today, the interior ice sheet would keep thinning for another 300 years and the ice sheet would take thousands of years to recover fully.

CONCLUSIONS

We used observed thinning rates below 2000 m elevation as the input to perturb the model to assess the inland propagation of the dynamic changes in the GIS. The model runs started from an initial present-day steady-state ice sheet with the perturbation applied for 10 years and then continued to 100 ka after the perturbations were switched off. The results show that the dynamic propagation penetrates deep into the interior ice sheet and that thinning is obvious within 10 years of the perturbation. The modeled thinning pattern over the ice sheet is in agreement with the observations: enhanced inland thinning mainly occurs in the western and eastern and, to some extent, the southeastern regions of the ice sheet. This implies that the strong mass loss since the early 2000s at the margins has had a dynamic impact on the entire GIS. The strongest impact for an isolated 10 year perturbation occurs at 300 years and it takes 10 ka for complete dynamic recovery. We conclude that the interior ice response to the changes at the ice-sheet margins is more rapid than generally expected and the dynamic impact will be sustained for a long period.

ACKNOWLEDGEMENTS

The research was supported by NASA ICESat project science and ROSES 10-CRYO10-0035. We thank two anonymous reviewers for helpful reviews.

REFERENCES

Azuma N and Goto-Azuma K (1996) An anisotropic flow law for ice-sheet ice and its implications. *Ann. Glaciol.*, **23**, 202–208

Bamber JL, Layberry RL and Gogineni SP (2001) A new ice thickness and bed data set for the Greenland ice sheet. 1. Measurement, data reduction, and errors. *J. Geophys. Res.*, **106**(D24), 33 773–33 780 (doi: 10.1029/2001JD900054)

Breuer B, Lange MA and Blindow N (2006) Sensitivity studies on model modifications to assess the dynamics of a temperate ice cap, such as that on King George Island, Antarctica. *J. Glaciol.*, **52**(177), 235–247 (doi: 10.3189/172756506781828683)

Budd WF (1971) Stress variations with ice flow over undulations. *J. Glaciol.*, **10**(59), 177–195

Budd WF and Warner RC (1996) A computer scheme for rapid calculations of balance-flux distributions. *Ann. Glaciol.*, **23**, 21–27

Dahl-Jensen D (1985) Determination of the flow properties at Dye 3, south Greenland, by borehole-tilting measurements and perturbation modelling. *J. Glaciol.*, **31**(108), 92–98

Glen JW (1958) The flow law of ice: a discussion of the assumptions made in glacier theory, their experimental foundation and consequences. *IASH Publ.* 47 (Symposium at Chamonix 1958 – *Physics of the Movement of the Ice*), 171–183

Greve R, Placidi L and Seddik H (2009) A continuum-mechanical model for the flow of anisotropic polar ice. In Hondoh T ed. *Physics of ice core records II*. Hokkaido University Press, Sapporo, 137–148 (Supplement Issue of Low Temperature Science 68)

Howat IM, Joughin IR and Scambos TA (2007) Rapid changes in ice discharge from Greenland outlet glaciers. *Science,* **315**(5818), 1559–1561 (doi: 10.1126/science.1138478)

Hutter K (1983) *Theoretical glaciology; material science of ice and the mechanics of glaciers and ice sheets*. D. Reidel, Dordrecht/ Terra Scientific, Tokyo

Huybrechts P, Letréguilly A and Reeh N (1991) The Greenland ice sheet and greenhouse warming. *Palaeogeogr., Palaeoclimatol., Palaeoecol.,* **89**(4), 399–412

Hvidberg CS, Dahl-Jensen D and Waddington ED (1997) Ice flow between the Greenland Ice Core Project and Greenland Ice Sheet Project 2 boreholes in central Greenland. *J. Geophys. Res.,* **102**(C12), 26 851–26 859 (doi: 10.1029/97JC00268)

Joughin I, Smith BE and Holland DM (2010) Sensitivity of 21st century sea level to ocean-induced thinning of Pine Island Glacier, Antarctica. *Geophys. Res. Lett.,* **37**(20), L20502 (doi: 10.1029/2010GL044819)

Li J and Zwally HJ (2011) Modeling of firn compaction for estimating ice-sheet mass change from observed ice-sheet elevation change. *Ann. Glaciol.*, **52**(59), 1–7 (doi: 10.3189/172756411799096321)

Li J, Jacka TH and Budd WF (1996) Deformation rates in combined compression and shear for ice which is initially isotropic and after the development of strong anisotropy. *Ann. Glaciol.*, **23**, 247–252

https://doi.org/10.3189/2012JoG11J187 Published online by Cambridge University Press

Mernild SH, Liston GE, Hiemstra CA and Steffen K (2009) Record 2007 Greenland ice sheet surface melt extent and runoff. *Eos,* **90**(2), 13–14 (doi: 10.1029/2009EO020002)

Nick FM, Vieli A, Howat IM and Joughin I (2009) Large-scale changes in Greenland outlet glacier dynamics triggered at the terminus. *Nature Geosci.,* **2**(2), 110–114 (doi: 10.1038/ngeo394)

Parizek BR and Alley RB (2004) Implications of increased Greenland surface melt under global-warming scenarios: ice-sheet simulations. *Quat. Sci. Rev.,* **23**(9–10), 1013–1027 (doi: 10.1016/j.quascirev.2003.12.024)

Paterson WSB (1994) *The physics of glaciers,* 3rd edn. Elsevier, Oxford

Pattyn F and 20 others (2008) Benchmark experiments for higher-order and full-Stokes ice sheet models (ISMIP-HOM). *Cryosphere,* **2**(2), 95–108 (doi: 10.5194/tc-2-95-2008)

Payne AJ, Vieli A, Shepherd A, Wingham DJ and Rignot E (2004) Recent dramatic thinning of largest West Antarctic ice stream triggered by oceans. *Geophys. Res. Lett.,* **31**(23), L23401 (doi: 10.1029/2004GL021284)

Price SF, Conway H and Waddington ED (2007) Evidence for late Pleistocene thinning of Siple Dome, West Antarctica. *J. Geophys. Res.,* **112**(F3), F03021 (doi: 10.1029/2006JF000725)

Price SF, Conway H, Waddington ED and Bindschadler RA (2008a) Model investigations of inland migration of fast-flowing outlet glaciers and ice streams. *J. Glaciol.,* **54**(184), 49–60 (doi: 10.3189/002214308784409143)

Price SF, Payne AJ, Catania GA and Neumann TA (2008b) Seasonal acceleration of inland ice via longitudinal coupling to marginal ice. *J. Glaciol.,* **54**(185), 213–219 (doi: 10.3189/002214308784886117)

Price SF, Payne AJ, Howat IM and Smith BE (2011) Committed sea-level rise for the next century from Greenland ice sheet dynamics during the past decade. *Proc. Natl Acad. Sci. USA (PNAS),* **108**(22), 8978–8983 (doi: 10.1073/pnas.1017313108)

Pritchard HD, Arthern RJ, Vaughan DG and Edwards LA (2009) Extensive dynamic thinning on the margins of the Greenland and Antarctic ice sheets. *Nature,* **461**(7266), 971–975 (doi: 10.1038/nature08471)

Wang WL and Warner RC (1999) Modeling of anisotropic ice flow in Law Dome, East Antarctica. *Ann. Glaciol.,* **29**, 184–190 (doi: 10.3189/172756499781820932)

Wang WL, Zwally HJ, Abdalati W and Luo S (2002a) Modeling of ice flow and internal layers along a flowline through Swiss Camp, West Greenland. *Ann. Glaciol.,* **34**, 303–308 (doi: 10.3189/172756402781817644)

Wang W, Warner RC and Budd WF (2002b) Ice-flow properties at Dome Summit South, Law Dome, East Antarctica. *Ann. Glaciol.,* **35**, 567–573 (doi: 10.3189/172756402781816924)

Zwally HJ and Giovinetto MB (2000) Spatial distribution of net surface mass balance on Greenland. *Ann. Glaciol.,* **31**, 126–132 (doi: 10.3189/172756400781820318)

Zwally HJ and 7 others (2005) Mass changes of the Greenland and Antarctic ice sheets and shelves and contributions to sea-level rise: 1992–2002. *J. Glaciol.,* **51**(175), 509–527 (doi: 10.3189/172756505781829007)

Zwally HJ and 11 others (2011) Greenland ice sheet mass balance: distribution of increased mass loss with climate warming; 2003–07 versus 1992–2002. *J. Glaciol.,* **57**(201), 88–102 (doi: 10.3189/002214311795306682)

MS received 2 September 2011 and accepted in revised form 13 January 2012